03

Interaction of a shock wave with a quartz sand partition

© S.V. Golovastov, G.D. Rublev, G.Y. Bivol, A.N. Parshikov, V.V. Golub

Joint Institute for High Temperatures, Russian Academy of Sciences,
125412 Moscow, Russia
e-mail: golovastov@yandex.ru

Received August 19, 2024
Revised October 21, 2024
Accepted November 26, 2024

The interaction of a shock wave propagating in a hydrogen-air mixture with a granular destructible partition was studied experimentally and numerically. The experiments were carrier out using a shock tube. The transverse dimensions of the diagnostic section were 40×40 mm. The initial pressure of the gas mixture varied from 10 kPA to 50 kPA. The molar excess of hydrogen varied from 0.3 to 0.5. The partition was made of quartz sand with a small addition of a clay-based binder. The experiments were carried out at Mach numbers of 2.09−2.88, while combustion in a hydrogen-air mixture was not considered. Numerical modeling of the destruction of the sand partition was carried out using smoothed particle hydrodynamics with interparticle contact algorithms of the Godunov type. Typical pressure oscillograms and the results of high-speed visualization of the interaction processes using the Schlieren technique are presented. The attenuation coefficients of the reflected and transmitted shock waves are determined. The results are aimed at reducing the shock wave effects of an explosion in a confined space.

Keywords: granular partition, shock wave, sand, wave attenuation, CSPH.

DOI: 10.61011/TP.2025.04.61203.257-24

Introduction

One of the crucial challenges of explosive safety consists in mitigating the effects of explosion of gas mixtures. Under shock-wave compression of a combustible mixture, one of the main factors is a degree of mixture compression and its heating to the self-ignition temperature. Most significantly, the ignition process is affected by a shock wave that is reflected from walls and partitions, resulting in almost double increase of the temperature, thereby reducing the ignition delay and increasing probability of ignition in a confined space.

In this case, the effective method of temperature reduction under shock-wave compression of the combustible mixture and, therefore, prevention of its ignition can be full or partial destruction of the partition from which the shock wave is reflected. Besides, the internal energy of the shock-compressed gas behind the shock wave is partially transferred to destruction of the partition and kinetic energy of flying submillimeter particles, which pose no serious threat [1]. Use of sand as a basic foundation of the destructible partition does not imply its use as strength structures, including as bearing supports of the constructions. However, use of sand with a small quantity of a binder can be used for manufacturing walls in framework buildings, protective and decorational screens.

Close attention is being currently paid to interaction between the shock wave and sand. Impact of the shock wave on sand was studied in the works [2–4], while a dynamic response and an unloading wave were studied in the works [5–8], and propagation of the shock wave in sand and equations of state are presented in the works [9,10]. In particular, the work [11] has studied interaction of the shock wave with a sand hillock, while the works [12,13] have studied tangential interaction of the shock wave with the surface of sand or dust. Deformation of a sandy soil and propagation of the explosion wave in dry sand subjected to a buried explosion have been studied in the work [14]. The dynamics of penetration of a projectile into the sandy soil has been studied in the work [15]. Specifically, it is worth noting several works on interaction and attenuation of the shock wave by granulated barrier [16,17]. A cycle of the works for attenuation of the shock wave with a falling explosion profile was experimentally and numerically carried out in Joint Institute for High Temperatures, RAS [18,19]. It also included determination of coefficients of attenuation of the shock wave depending on the thickness of the destructible screen and its position in relation to a closed end of the shock tube.

Together with the destructible partition, efficiency of attenuation of intensity of the shock wave was also demonstrated by perforated plates [20–27], including packages of the perforated plates [28]. Wire meshes or woven materials can also be effective in attenuation of the shock wave [29–31]. The work [30] has shown that in interaction with the perforated partition an amplitude of the reflected shock wave can decrease in 2−5 times. The work [32] has considered interaction of the shock wave with drops of a bubble liquid. The reflected shock wave can be attenuated by using polyurethane [33] or by using multi-layer partitions

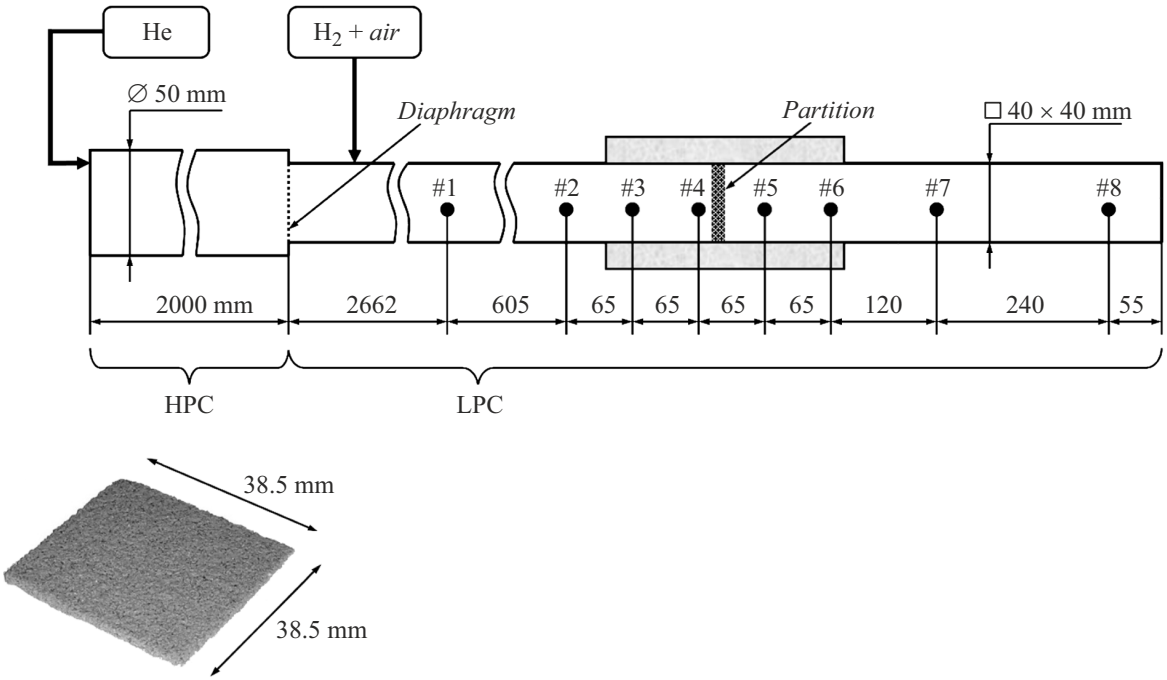

Figure 1. Setup of the experimental bench and photograph of the sand partition. #1 – #8 — pressure sensors; HPC — high-pressure chamber; LPC — low-pressure chamber.

with a granular filler [34]. Using the shock tube [35] for studying impact of the shock waves with a constant profile of pressure is a convenient tool for studying processes of attenuation of intensity of the shock waves.

By analyzing the given review, it can be concluded that the majority of the works are dedicated to attenuation of a transmitted shock wave rather than the reflected one, as shown in the review [36]. However, propagation of the shock wave directly in the combustible mixture and its reflection from protection means can exactly result in local repeated increase of the temperature. As shown in the work [37], with reflection of the shock from the destructible partition, self-ignition of the combustible mixture can happen.

The present work has considered interaction of the shock wave with the destructible sand partition for the Mach numbers, at which there was no self-ignition in the hydrogen-air mixture. It could exclude impact of additional increase of pressure, which could introduce off-design corrections to measurements results. The present work was aimed at obtaining the values of coefficients of attenuation of the reflected and transmitted shock waves, which are determined as ratios of pressure at their front to pressure at the front of the shock wave interacting with the destructible sand partition.

1. Investigation procedure

1.1. Experimental setup

The shock tube was used in the present work. The setup of the experimental bench is presented in Fig. 1. The high-pressure chamber of a length of 2000 mm with an internal diameter of 50 mm was filled with helium. The low-pressure chamber of the total length of 3942 mm with a rectangular internal section of40×40 mm was filled with the hydrogen-air mixture. The chambers were partitioned by an aluminum or copper diaphragm of the various thickness: 80, 100, 150 μm for the aluminum diaphragms and 100, 120 μm for the copper ones. With rupture of the notched diaphragm, the low-pressure chamber has the shock wave formed.

The sand partition was made of quartz sand with the binder based on blue clay in a weight ratio sand : clay : water = 15 : 1 : 2. The size of sand granules was 0.1 – 0.4 mm. Fig. 1 shows a photograph of the sand partition. The transverse sizes of the partition were on average 38.5×38.5 mm. Thus, there were gaps between the walls of the low-pressure chamber and facets of the sand partition. The gaps provided unhindered flow of the hydrogen-air mixture or air when filling the chamber or when evacuating it. The sand partition was set up vertically on the lower wall of a diagnostic section of the low-pressure chamber. The thickness of the partition was on average 2.6 mm, so was its weight — 4.5 g. In order to avoid falling of the partition during vacuuming and filling it was fixed in its upper part by a wire shackle of the thickness of 700 μm and of the length of 2 mm, which flew away with the partition during interaction with the shock wave. The partition was place in the low-pressure chamber at the distance of 8 mm from the pressure sensor #4 and at the distance of 537 mm from the closed end of the low-pressure chamber. This length made it possible to neglect impact of the shock waves reflected from the closed end, on the dynamics of destruction of the partition.

Propagation of the incident, reflected and transmitted shock waves was recorded by the piezoelectric pressure sensors PCB 111A and 113B. The pressure sensors #1 – #4 recorded the incident shock wave and the shock wave reflected from the sand partition. The pressure sensors #5 – #8 recorded the shock wave passed through the partition. The error of determination of the Mach number did not exceed 3 %.

The high-speed digital camera Phantom Veo 710 and the IAB-451 Schlieren device were used to record the shock, reflected and transmitted shock waves and the dynamics of the partition. The Foucoult knife was used. The recording frequency was 68 000–90 000 fps (frames per second) with resolution 512 × 128 and the exposure time of 1 μs. A 35 W xenon lamp provided continuous illumination. Polymethyl methacrylate glasses were used and they are characterized by resistance and restorability after impact by the granules of the sand partition.

The hydrogen-air mixture was prepared in advance in a 3-l separate vessel according to partial pressures and mixed with a brushless fan. The maximum pressure in the mixing vessel was 0.6 MPa. Three mixtures with the hydrogen molar excess $\varphi = 0.3$, 0.4 and 0.5 were used. The initial pressure of the hydrogen-air mixture in the low-pressure chamber varied from 10 to 50 kPa. Table 1 shows the parameters of the used gas mixtures.

In order to determine the time interval in which the pressure behind the reflected shock wave does not vary, preliminary experiments were performed, in which the shock wave interacted with the fixed aluminum unit. The unit was placed so as its front wall was in the same position as the sand partition. Fig. 2 shows the typical Schlieren photographs of interaction of the shock wave with the fixed metal wall. The shock wave (SW) propagated from the left to the right (0 μs; 58.8 μs). The frames 117.6 μs and further show propagation of the reflected shock wave (RSW) from the right to the left.

Fig. 3 shows the respective pressure oscillograms obtained in the same experiment. The figure also shows the values of the pressure behind the incident shock wave (P_2^*) and behind the reflected shock wave (P_5^*), which are calculated in single-dimensional approximation by the equations of the gas dynamics:

$$\frac{P_2^*}{P_1} = \frac{2\gamma M_1^2 - (\gamma - 1)}{\gamma + 1}, \qquad (1)$$

Table 1. Parameters of the hydrogen-air mixtures depending on the molar excess of hydrogen φ

φ	Molar composition	μ, g/mol	c, m/s
0.3	$0.3H_2 + 0.5O_2 + 1.88N_2$	26	365
0.4	$0.4H_2 + 0.5O_2 + 1.88N_2$	25	372
0.5	$0.5H_2 + 0.5O_2 + 1.88N_2$	24	380

Note: μ — the molar weight; c — the sound velocity.

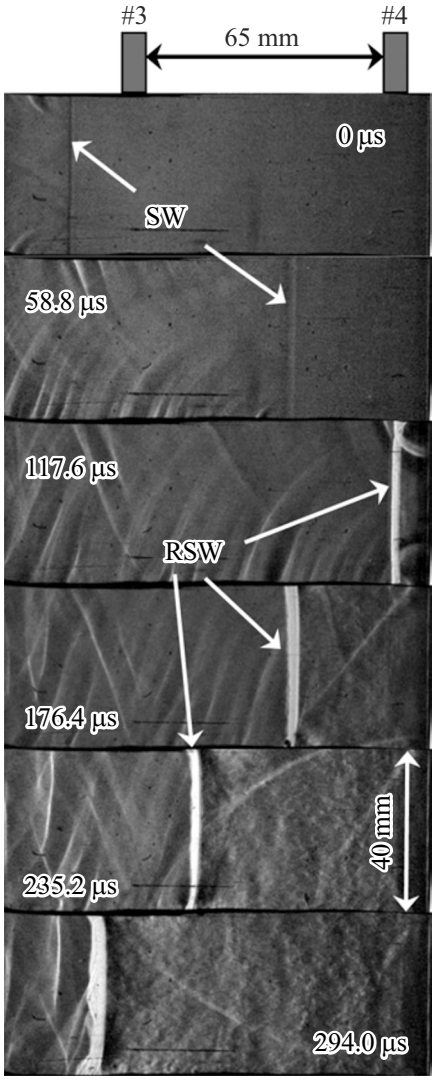

Figure 2. Schlieren photographs of interaction of the shock wave with the fixed aluminum unit. Composition $\varphi = 0.3$; the initial pressure 20 kPa; the Mach number $M_1 = 2.10$. SW — the shock wave; RSW — the reflected shock wave.

$$\frac{P_5^*}{P_1} = \frac{2\gamma M_1^2 - (\gamma - 1)}{\gamma + 1} \times \frac{(3\gamma - 1)M_1^2 - 2(\gamma - 1)}{(\gamma - 1)M_1^2 + 2}. \qquad (2)$$

Here $\gamma = 1.4$ — the adiabatic index for the mixture of diatomic gases, M_1 — the Mach number of the shock wave. As it is clear from Fig. 3, the period at which the pressure behind the reflected shock wave as recorded by the pressure sensors #3 and #4 does not vary, is 2 ms. The pressure behind the falling and incident shock waves corresponds to the design value as per the equations (1) and (2).

1.2. Numerical modeling

Destruction of the sand partition by the shock wave was numerically modelled by a smoothed particle hydrodynamics method. For modelling, the contact smoothed particle method of the Godunov type — the so-called Smoothed

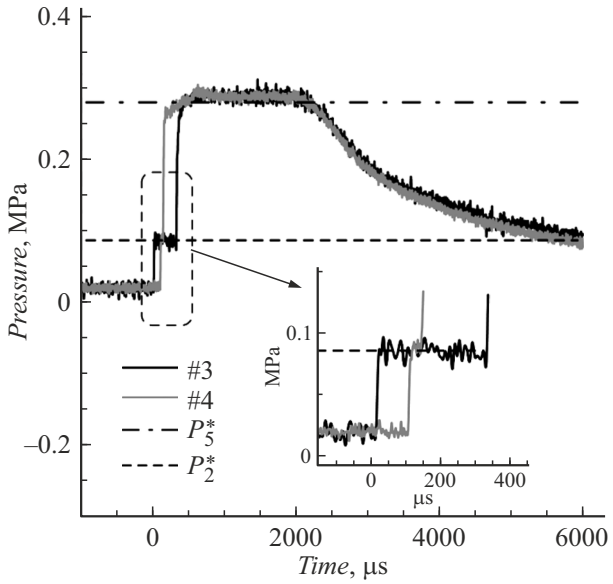

Figure 3. Pressure oscillograms in interaction of the shock wave with the fixed aluminum unit. Composition $\varphi = 0.3$; the initial pressure 20 kPa; the Mach number $M_1 = 2.10$; the pressure sensors #3 and #4.

Particle Hydrodynamics Using Interparticle Contact Algorithms (abbreviated as CSPH). The method is detailed in the work [38]. The initial size of the SPH-particles was 70.7 μm. The total number of the SPH particles in the design area was 4.16 millions.

The modeling was performed in the two-dimensional setup. The sizes of the design are were 2.5 m along the horizontal axis x and 8 mm along the vertical axis y. A periodic boundary condition was specified along the axis y. The boundary condition at the right boundary of the design area is a fixed rigid wall. The sand partition was initially placed at the distance of 0.4 m from the right boundary of the design area. A boundary condition at the left boundary of the design area is a piston moving at the speed corresponding to the velocity behind the front of the shock wave. The state of the gas to the left of the partition corresponds to the state behind the front of the shock wave with the respective Mach number. The gas is considered to be ideal with the adiabatic exponent $\gamma = 1.4$.

The sand was specified as randomly packed round grains with the diameter of 0.3 mm. The clay was specified as random inclusions. The partition was specified so as its average density was 1170 kg/m^3 taking into account porosity. The sand and the clay were modeled without using the strength model. It was assumed that the grains interact with each other without friction.

The sand and the clay were modeled using the linear equation of state $P = c_0^2(\rho - \rho_0)$, where P — the pressure, c_0 — the volume sound velocity, ρ_0 — the initial density, ρ — the current density. Parameters of the equation of state of quartz sand and clay used in numerical modeling are shown in Table 2.

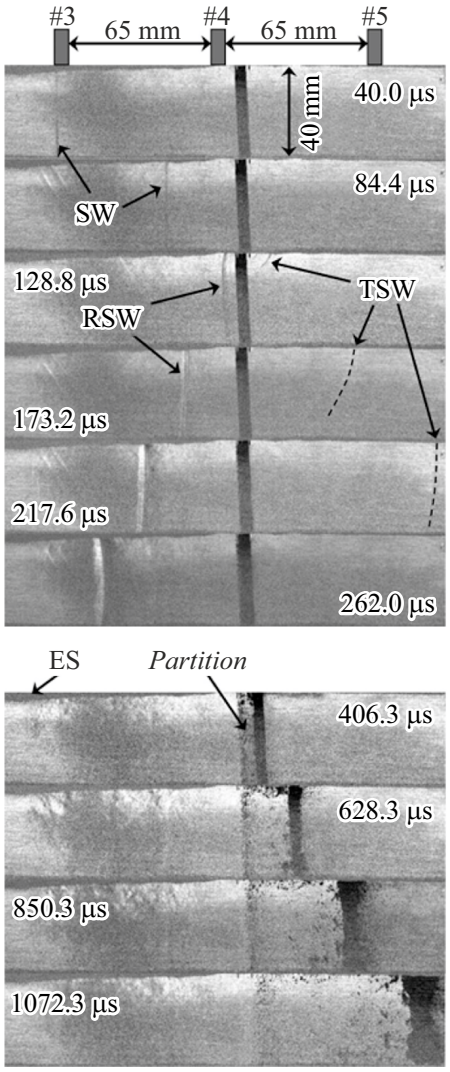

Figure 4. Schlieren photographs of interaction of the shock wave with the sand partition. Composition $\varphi = 0.3$; the initial pressure 20 kPa; the Mach number $M_1 = 2.29$. SW — the shock wave; RSW — the shock wave reflected from the partition; TSW — the passed shock wave; ES — the external sealant shadow.

Table 2. Parameters of the equation of state of quartz sand and clay in numerical modeling

Component	ρ_0, kg/m^3	c_0, m/s
Sand	2300	5500
Clay	1200	1000

Note: c_0 — the volume sound velocity; ρ_0 — the initial density.

2. Experimental results

Fig. 4 exemplifies results of interaction of the shock wave (SW) with the sand partition. The results are given for the mixture $\varphi = 0.3$ at the initial pressure of 20 kPa and the Mach number of 2.29 for the incident shock wave.

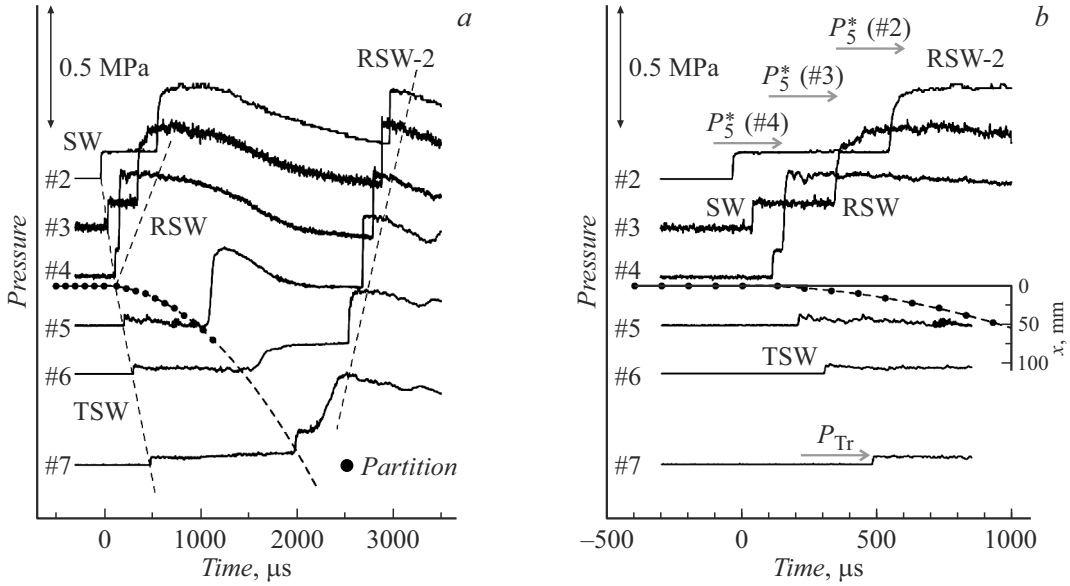

Figure 5. Pressure oscillograms and paths of the partition and the shock waves: the incident (SW), transmitted (TSW), reflected from the partition (RSW) and from the butt end of the shock tube (RSW-2). *a* — the time interval $-700-3500\,\mu$s; *b* — the time interval $-500-1000\,\mu$s. Composition $\varphi = 0.3$; the initial pressure 20 kPa; the Mach number $M_1 = 2.29$; P_5^* — the design value of pressure behind the reflected shock wave in the position of the pressure sensors #2, #3 and #4.

After interaction of the shock wave with the partition, the reflected shock wave (RSW) is formed, wherein the front at the upper facet slightly lags behind the front at the lower facet ($128.8\,\mu$s). Slight curvature of the front of the shock wave is due to the gap between the partition and the upper facet of the diagnostic section. At the same time with reflection of the shock wave there is a recorded shock wave (TSW) transmitted through this gap between the partition and the upper wall ($128.8\,\mu$s). As it is clear, at the time moment of $217.6\,\mu$s, the front of the transmitted shock wave become flatter. The frames $406.3-1072.3\,\mu$s show a process of destruction of the partition into fragments.

Fig. 5, *a* show respective oscillograms of pressure for interaction of the shock wave with the sand partition. The pressure sensors #2, #3 and #4 recorded the incident and reflected shockwaves, while the pressure sensors #5, #6 and #7 recorded the transmitted shock wave. The vertical intervals between the oscillograms correspond to the distance between the pressure sensors. Fig. 5 also shows an initial position of the sand partition and a path of the collapsing partition in relation to the pressure sensors. Fig. 5, *a* show by dashed lines the paths of motion of the incident, reflected and transmitted shock waves.

Fig. 5, *b* shows the same oscillograms with an extended time scale. The arrows shows the design values of the pressures P_5^* when reflecting from the fixed metal wall, as calculated as per the equation (2). As it is clear from Fig. 5, *b*, the pressure behind the reflected shock wave is below this design value in the position of the pressure sensors #2, #3 and #4, wherein when moving away from the partition, the amplitude of the reflected shock wave decreases. The amplitude of the transmitted shock wave is in several times less than the amplitude of the incident shock wave. At the same time, the profile is variable due to transients when forming the shock wave during transmitting through the gap.

As it is clear from Fig. 5, the path of the partition within the recording area is approximated by a parabolic function, which generally corresponds to uniformly accelerated motion. For the case under consideration, the parabolic equation of motion of the partition is as follows

$$x = 0.54 \cdot 10^5 t^2, \tag{3}$$

where displacement x of the relative initial position is determined in meters, so is the time in seconds (Fig. 5, *b*). Thus, the acceleration of the partition determined by the motion path is $1.08 \cdot 10^5$ m/s^2. When the partition is displaced and at the moments of its transmission through the pressure sensors #5, #6 and #7, there is recorded secondary increase of the pressure behind the front of the transmitted shock wave. The moments of pressure increase correspond to the expected parabolic approximation (3) of the partition motion.

On the other hand, the acceleration of the partition can be evaluated by a force acting on the partition by the shock-compressed gas:

$$a = (P_5 - P_{Tr})S/m, \tag{4}$$

where P_5 — the pressure behind the reflected shock wave, P_{Tr} — th pressure behind the transmitted shock wave, S — the partition area, m — the partition weight. Since the gas velocity behind the reflected shock wave is considered to be zero, action of pulse by the shock-compressed gas

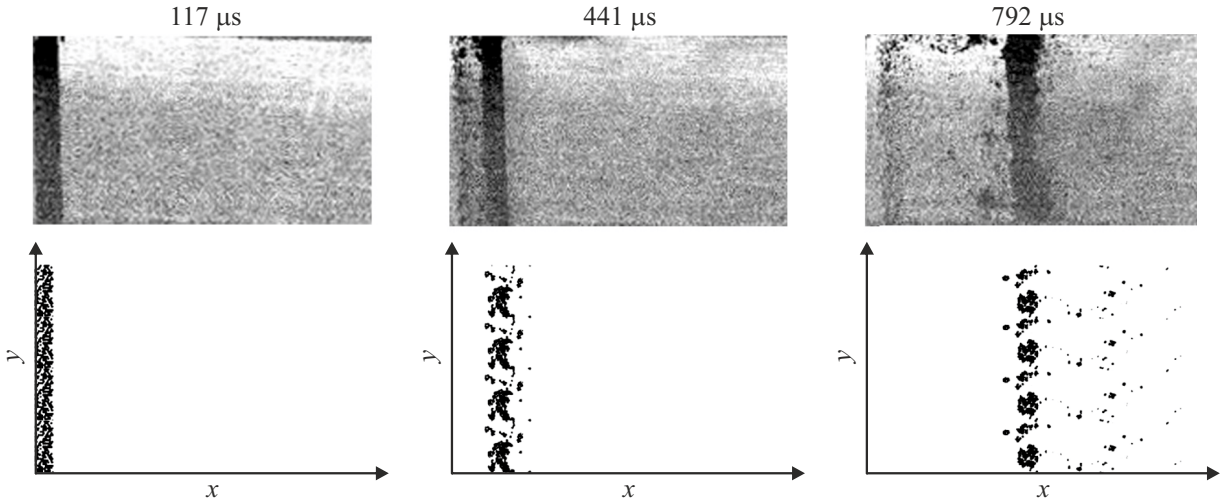

Figure 6. Evolution of the partition: the experiment (top) and modeling (bottom).

was neglected. Determination of the amplitude of the pressure P_{Tr} is shown in Fig. 5, *b*. Using the data of Fig. 5, the acceleration can be determined by means of the equation (4). It was $a = 1.25 \cdot 10^5$ m/s^2, which slightly exceeds the measured value. This difference is explained by the fact that during displacement of the partition and with presence of the gaps between the partition and the chamber walls there is expansion of the shock-compressed gas and, respectively, pressure decrease. This is why the pressure behind the shock wave reflected from the partition has a falling profile and the pressure decreases in almost two times in 2 ms after compression (Fig. 5, *a*).

Within the interval 2500–3000 μs (Fig. 5, *a*), the pressure sensors record the shock wave reflected from the rigid wall of the shock tube. This reflected shock wave, which also has the falling profile, goes to the original location of the partition in 2.5 ms after impact of the incident shock wave.

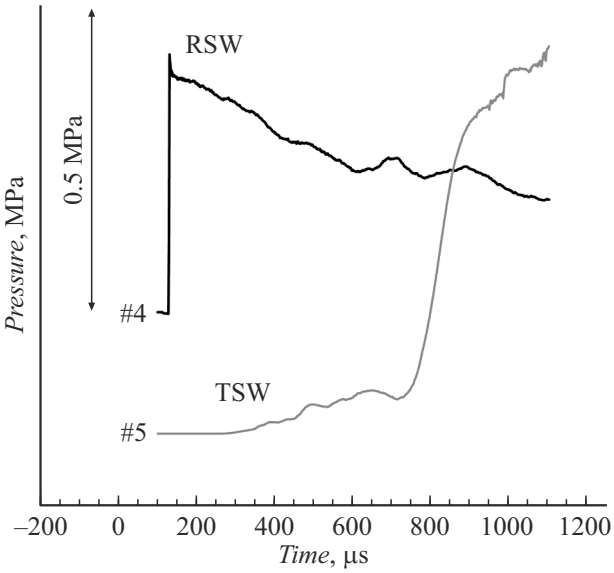

Figure 7. Dependences of pressure on time #4 (in front of the partition) and #5 (behind the partition), computational modeling. RSW — the shock wave reflected from the partition; TSW — the passed shock wave.

3. Computational modeling results

The fly-off dynamics of the sand partition has been computationally modeled with the Mach number of the shock wave $M_1 = 2.29$ in accordance with the specified conditions for the experimental data of the figures 4 and 5. Fig. 6 at the bottom shows the results of computational modeling of evolution of the partition. As it is clear from Fig. 6, a small part of the partition is moved away by flow forward following the shock wave transmitted through the gaps. Fig. 6 at the top shows for comparison the respective Schlieren photographs that are obtained experimentally. It is clear that the modeling well reproduces the velocity of motion of the sand partition and its destruction. Based on the results of modeling, the approximate parabolic equation of motion of the partition is as follows:

$$x = 0.5 \cdot 10^5 t^2, \tag{5}$$

where the displacement x is also determined in relation of the original position in meters, while the time is determined in seconds from the moment of arrival of the shock wave to the partition. Thus, the acceleration of the partition as determined in computational modeling by the motion path (5), is equal to 10^5 m/s^2, which is comparable to the experimentally measured value.

Fig. 7 shows the computationally modeled dependences of pressure on time on the sensors #4 (in front of the

partition) and #5 (behind the partition). It is clear that the modeling results agree with the experimental observations shown in Fig. 5 for the same pressure sensors #4 and #5.

4. Generalizing data

Fig. 8 shows the values of the ratio of pressure at the front shock wave reflected from the sand partition P_5 to the design value of P_5^* when reflecting from the hard wall depending on a distance of the front of the reflected shock wave to the partition. The initial pressure of the mixture in the low-pressure chamber is selected to be a parameter. The results are combined in all the compositions, as separating the results by the mixture compositions has not resulted in substantial difference in the numerical values. The Mach number ranges for each initial pressure are shown in Table 3. As it is clear from Fig. 8, the maximum attenuation of the reflected shock wave was obtained at the higher initial pressure. Thus, for example, at the distance of 8 mm to the partition there was almost no recorded attenuation of the reflected shock wave at the initial pressure of 10 kPa, whereas at the initial pressure of 50 kPa the attenuation was 0.75. With the initial pressures 20−40 kPa, attenuation of the reflected shock wave varied within the range 0.90−0.75, respectively.

When moving away to the distance of 73 mm to the sand partition, the amplitude of pressure at the front of the reflected shock wave decreased to 0.85−0.60 in relation to the design value at the initial pressure of 20−50 kPa. With the initial pressure of 10 kPa, the pressure behind the reflected shock wave was still almost unvaried. Reduction of the pressure to 0.9 of the design value was recorded only at the distance of 138 mm to the sand partition. Also, at the

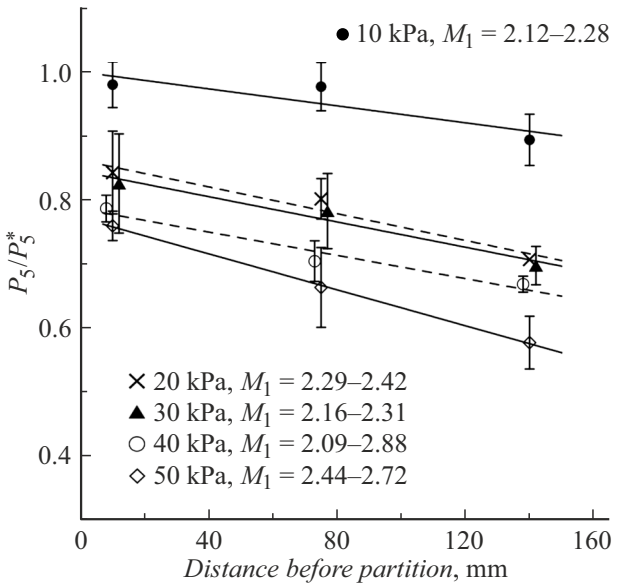

Figure 8. Ratio of the pressure at the front shock wave reflected from the sand partition P_5 to the design value of P_5^* when reflecting from the hard wall.

Table 3. Mach numbers of the shock wave M_1 and linear dependences of the pressure ratio P_5/P_5^* behind the reflected shock wave on the distance x to the partition

Initial pressure	M_1	P_5/P_5^*
10 kPA (●)	2.12−2.28	$1.00-0.00066\,\text{mm}^{-1}\cdot x$
20 kPA (×)	2.29−2.42	$0.86-0.00104\,\text{mm}^{-1}\cdot x$
30 kPA (▲)	2.16−2.31	$0.84-0.00105\,\text{mm}^{-1}\cdot x$
40 kPA (○)	2.09−2.88	$0.80-0.00110\,\text{mm}^{-1}\cdot x$
50 kPA (◇)	2.44−2.72	$0.77-0.00140\,\text{mm}^{-1}\cdot x$

distance of 138 mm to the partition, the reduction of the pressure was already 0.75−0.55 with the initial pressures 20−50 kPa.

As it is clear from Fig 8, the obtained dependences of attenuation of the pressure on the distance to the partition are of a linear type at the distance of up to four calibers of the shock tube. Fig. 3 shows linear approximations of the respective pressure ratios behind the reflected shock wave depending on the distance to the partition. At the same time, a coefficient in front of the variable x, which corresponds to an line slope of Fig. 8, is the greater, when the initial pressure is greater: $0.00066\,\text{mm}^{-1}$ with the initial pressure of 10 kPa, $0.00140\,\text{mm}^{-1}$ with the initial pressure of 50 kPa.

Besides partial effluence of the shock-compressed gas through the gaps between the sand partition and the walls of the low-pressure chamber, this impact of the initial pressure on intensity attenuation of the reflected shock wave may be due to displacement and destruction of the san partition. This displacement is determined by action by the shock-compressed gas, which is determined as a product of pressure to the partition area, as provided in the equation (4).

Fig. 9 shows the values of the coefficient of attenuation of the transmitted shock wave depending on the distance of its front to the partition. The range of the Mach numbers M_1 of the shock waves is also shown in Table 3. As it is clear from Fig. 9, the pressure at the front of the transmitted shock wave varies non-monotonically. This variation is explained by the fact that propagation of the transmitted shock wave is a multi-stage process. At first, a spherical shock wave is formed when the shock-compressed gas flows out through the gaps between the partition and the chamber walls. Then, after being repeatedly reflected from the low-pressure chamber walls the spherical shock wave transfers into a flat shock wave. Depending on the dynamics of destruction of the partition, especially along its perimeter, the pressure at the front of the shock wave can either decrease (the spherical shock wave has not become the flat shock wave) or increase (the shock wave front takes the flat form). Besides, in accordance with the data of Fig. 9, at the distance of 122−242 mm to the partition

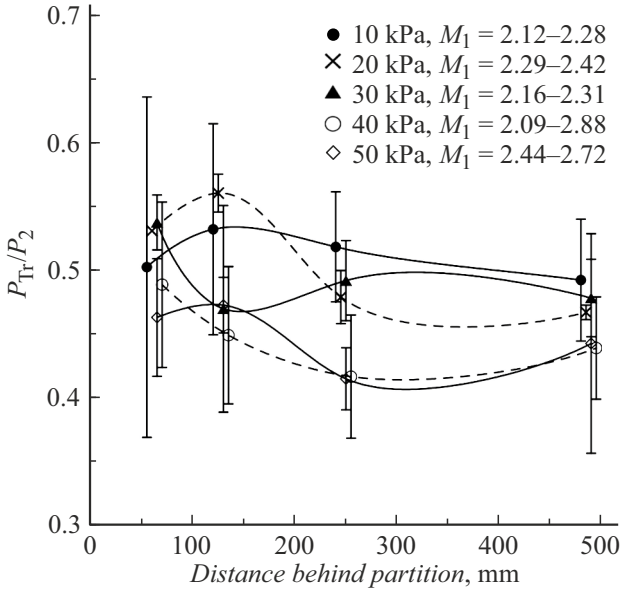

Figure 9. Ratio of the pressure at the front of the shock wave P_{Tr} transmitted through the partition to the pressure P_2 at the front of the incident shock wave.

the transmitted shock wave (0.45−0.62) at the lower initial pressure 10−20 kPa attenuates less than the shock wave (0.37−0.50) at the higher initial pressure 40−50 kPa. This difference in attenuation of the transmitted shock wave may be due to viscose effects in the gaps between the partition and the low-pressure chamber walls at the initial stage of formation of the transmitted shock wave until the moment of partial or full destruction of the sand partition. At the distance of 482 mm behind the partition the difference in the pressures at the front of the transmitted shock wave becomes minimal, so the spread of the average values is 10 %. Unlike the reflected shock wave, the obtained data are insufficient for providing a formula of attenuation of the transmitted shock wave.

Conclusion

Based on the provided experimental data, it can be concluded that the use of the destructible sand partition results in attenuation both of the transmitted as well as the reflected shock wave. Within the range of the Mach numbers $M_1 = 2.09 - 2.72$ of the incident shock wave the coefficients of attenuation of the reflected shock wave varied from 0.75 to 1 depending on the initial pressure. When moving away from the partition, the attenuation was already 0.6−0.9.

Action of the destructible partition for reduction of the pressure at the front of the reflected shock wave is the more efficient, when the initial pressure of the gas mixtures is greater. If at the initial pressure of 10 kPa the ratio of the pressure at the front of the reflected shock wave to the design value when being reflected from the rigid wall was still at least 0.9, at the initial pressure of 50 kPa it was already 0.6. This influence of the initial pressure is related to the higher density of the gas affecting the partition and setting it in motion. This motion results in unloading of the shock-compressed gas and, therefore, in reduction of the pressure by the incident shock wave.

Using the smoothed particle hydrodynamics method makes it possible with satisfactory accuracy to model the process of destruction of the sand partition as affected by shock wave which is incident thereto. As the calculation results have shown, the partition dynamics coincides with the dynamics experimentally determined by the Schlieren method.

The experiments have shown that the transmitted shock wave is formed in many stages, thereby explaining that the pressure at its front non-monotonically changes along an axis of the pressure channel, whereas the average value of the pressure attenuation coefficient at the smaller initial pressures 10−20 kPa is higher than at the higher initial pressures 40−50 kPa.

Funding

The study was supported by the Russian Science Foundation grant № 23-21-00251 (https://rscf.ru/project/23-21-00251/).

Conflict of interest

The authors declare that they have no conflict of interest.

References

[1] A.G. John, K.D. Gardner, F.K. Lu, V.V. Volodin, S.V. Golovastov, V.V. Golub. In: Proc. 25th ISSW (Bangalore, India, 2005), https://arc.uta.edu/publications/cp_files/10044.pdf
[2] X.M. Li, M. Wang, X. Guo, Y.J. Li, Y.C. Peng. Appl. Mech. Mater., **556**, 3187 (2014). DOI: 10.4028/www.scientific.net/AMM.556-562.3187
[3] H. Lv, Z. Wang, J. Li. Int. J. Multiphase Flow., **89**, 255 (2017). DOI: 10.1016/j.ijmultiphaseflow.2016.07.019
[4] A.D. Resnyansky, N.K. Bourne. AIP Conf. Proc., **706** (1), 1474 (2004). DOI: 10.1063/1.1780517
[5] M. Arlery, M. Gardou, J.M. Fleureau, C. Mariotti. Int. J. Impact Eng., **37** (1), 1 (2010). DOI: 10.1016/j.ijimpeng.2009.07.009
[6] C.H. Braithwaite, J.I. Perry, N.E. Taylor, A.P. Jardine. Appl. Phys. Lett., **103** (15), 154103 (2013). DOI: 10.1063/1.4824764
[7] S.K. Dwivedi, L. Pei, R. Teeter. J. Appl. Phys., **117** (8), 085902 (2015). DOI: 10.1063/1.4913479
[8] J.W. LaJeunesse, M. Hankin, G.B. Kennedy, D.K. Spaulding, M.G. Schumaker, C.H. Neel, J.P. Borg, S.T. Stewart, N.N. Thadhani. J. Appl. Phys., **122** (1), 015901 (2017). DOI: 10.1063/1.4990625
[9] D.J. Chapman, K. Tsembelis, W.G. Proud. AIP Conf. Proc., **845** (1), 1445 (2006). DOI: 10.1063/1.2263596
[10] A.D. Resnyansky, S.A. Weckert. J. Phys.: Conf. Series, **500** (19), 192016 (2014). DOI: 10.1088/1742-6596/500/19/192016

[11] Y. Sugiyama, M. Izumo, H. Ando, A. Matsuo. Shock Waves, **28**, 627 (2018). DOI: 10.1007/s00193-018-0813-5
[12] B. Fletcher. J. Physics D: Appl. Phys., **9** (2), 197 (1976). DOI: 10.1088/0022-3727/9/2/009
[13] R.T. Paton, B.W. Skews. In: Proc. 31st ISSW 2: Applications, **31**, 673 (2019). DOI: 10.1007/978-3-319-91017-8_84
[14] L. Guan, J. Zhang, J. Li, Y. Ding, Y. Wang, Q. Lu. Int. J. Impact Eng., **188**, 104935 (2024). DOI: 10.1016/j.ijimpeng.2024.104935
[15] S.I. Gerasimov, Yu.F. Travov, A.G. Ioilev, V.V. Pisetsky, N.N. Travova, A.P. Kalmykov, S.A. Kapinos, N.V. Lapichev, Yu.I. Faikov. Tech. Phys., **3**, 300 (2022). DOI: 10.21883/TP.2022.03.53261.275-21
[16] A. Britan, T. Elperin, O. Igra, J.P. Jiang. AIP Conf. Proc., **370** (1), 971 (1996). DOI: 10.1063/1.50571
[17] A. Britan, G. Ben-Dor, O. Igra, H. Shapiro. Int. J. Multiphase Flow, **27** (4), 617 (2001). DOI: 10.1016/S0301-9322(00)00048-3
[18] O.A. Mirova, A.L. Kotelnikov, V.V. Golub, T.V. Bazhenova, A.N. Parshikov. High Temp., **54**, 716 (2016). DOI: 10.1134/S0018151X16050199
[19] O.A. Mirova, A.L. Kotel'nikov, V.V. Golub, T.V. Bazhenova. High Temp., **53**, 155 (2015). DOI: 10.1134/S0018151X15010174
[20] I.I. Anik'ev, M.I. Mikhailova, E.A. Sushchenko. Int. Appl. Mech., **42**, 1307 (2006). DOI: 10.1007/s10778-006-0202-0
[21] A. Britan, A.V. Karpov, E.I. Vasilev, O. Igra, G. Ben-Dor, E. Shapiro. J. Fluids Eng. **126** (3), 399 (2004). DOI: 10.1115/1.1758264
[22] C.V.P. Kumar, C.H. Reddy, L.R. Sai, K.D. Kumar, S.R. Nagaraja. IOP Conf. Series: Mater. Sci. Eng., **225**, 012059 (2017). DOI: 10.1088/1757-899X/225/1/012059
[23] G.S. Langdon, G.N. Nurick, N.J. Du. Plessis. Eng. Structur., **33** (12), 3537 (2011). DOI: 10.1016/j.engstruct.2011.07.017
[24] H. Onodera. Exp. Fluids, **24** (3), 238 (1998). DOI: 10.1007/s003480050170
[25] T. Schunck, D. Eckenfels. SN Appl. Sci., **3**, 1 (2021). DOI: 10.1007/s42452-021-04720-3
[26] O. Ram, G. Ben-Dor, O. Sadot. Exp. Therm. Fluid Sci., **92**, 211 (2018). DOI: 10.1016/j.expthermflusci.2017.11.014
[27] B. Skews. Exp. Fluids, **39**, 875 (2005). DOI: 10.1007/s00348-005-0023-7
[28] S. Golovastov, A. Mikushkin, A. Mikushkina, Y. Zhilin. Exp. Fluids, **63** (6), 97 (2022). DOI: 10.1007/s00348-022-03451-4
[29] Y. Andreopoulos, S. Xanthos, K. Subramaniam. Shock Waves, **16**, 455 (2007). DOI: 10.1007/s00193-007-0082-1
[30] T. Schunck, M. Bastide, D. Eckenfels, J.F. Legendre. Shock Waves, **31** (6), 511 (2021). DOI: 10.1007/s00193-021-01004-y
[31] W. Xiao, M. Andrae, N. Gebbeken. Eng. Structur., **213**, 110574 (2020). DOI: 10.1016/j.engstruct.2020.110574
[32] V.S. Surov. Tech. Phys., **46** (6), 662 (2001). DOI: 10.1134/1.1379630.
[33] G.Y. Bivol, V.V. Volodin, Yu.V. Zhilin, V.M. Bocharnikov. High Temp., **57** (1), 130 (2019). DOI: 10.1134/S0018151X19010024
[34] M. Rahmani, A.N. Oskouei, A.M. Petrudi. Defence Tech., **17** (5), 1660 (2021). DOI: 10.1016/j.dt.2020.09.004
[35] I.A. Znamenskaya, E.A. Karnozova. Tech. Phys., **69** (6), 791 (2024). DOI: 10.61011/TP.2024.06.58820.45-24
[36] O. Igra, J. Falcovitz, L. Houas, G. Jourdan. Progr. Aerospace Sci., **58**, 1 (2013). DOI: 10.1016/j.paerosci.2012.08.003
[37] S.V. Golovastov, G.Yu. Bivol, F.S. Kuleshov, V.V. Golub. Tech. Phys. Lett., **50** (3), 41 (2024). DOI: 10.61011/PJTF.2024.05.57185.19763
[38] A.N. Parshikov, S.A. Medin. J. Comp. Phys., **180**, 1 (2002). DOI: 10.1006/jcph.2002.7099

Translated by M.Shevelev